ELSEVIER

Journal of Nuclear Materials 277 (2000) 217–225

journal of nuclear materials

www.elsevier.nl/locate/jnucmat

TEM study of the aging of palladium-based alloys during tritium storage

S. Thiébaut[a], B. Décamps[b,*], J.M. Pénisson[c], B. Limacher[a], A. Percheron Guégan[b]

[a] *CEA/DAM, Service EMN, Centre d'Etudes de Valduc, 21120 Is sur Tille, France*

[b] *Laboratoire de Chimie Métallurgique des Terres Rares, UPR 209 du CNRS, Groupe des Laboratoires de Vitry-Thiais, 2-8 rue Henri Dunant, 94320 Thiais cedex, France*

[c] *CEA-Grenoble/Département de Recherche Fondamentale sur la Matière Condensée/SP2M/ME, 85X, F-38041 Grenoble cedex, France*

Received 15 March 1999; accepted 16 July 1999

Abstract

The defects (^{3}He bubbles, dislocations, dislocation loops, clusters of self-interstitial atoms) formed during aging of palladium tritides are analyzed using a combination of transmission electron microscopy techniques. Their evolution under aging together with the effect of the metallic substitution by Rh or Pt is investigated. A comparison with the results previously obtained from X-ray and neutron scattering experiments is also performed.

PACS: 61-72.-y; 61-72.-Ff; 61-72.-Ji; 61-72.-Qq

1. Introduction

Tritium is an essential element for the future thermonuclear energy production. Due to its radioactivity and its high mobility, its handling and storage need to be well mastered.

As other metals and alloys (uranium, lanthanum-nickel based alloys,...), palladium and its alloys are commonly used for hydrogen isotopes processing and storage [1,2]. Due to its high ability to retain the ^{3}He generated by tritium decay, palladium appears as a very good candidate for use in tritium facilities.

As a part of a general program to get a better knowledge of aging of some metal tritides, we have been investigating the partial substitution of palladium by rhodium or platinum.

Helium created by tritium decay in metal tends to precipitate into bubbles. At room temperature, bubble growth occurs by athermal mechanisms implying Self-Interstitial Atoms (SIA) formation and dislocation loop punching resulting in a dislocation network [3–6].

The object of this paper is to study by a combination of different transmission electron microscopy (TEM) techniques the microstructural evolution of the alloys during aging and to compare the effects of the metallic substitution.

2. Experimental procedure

2.1. Specimen preparation

Palladium specimens were prepared from 0.13 mm thick foils supplied by the Aldrich Company. 1 mm thick slices of $Pd_{90}Pt_{10}$ (% at.) and $Pd_{90}Rh_{10}$ (% at.) alloys were cut out from bars ($\Phi = 1$ cm, $L = 10$ cm) supplied by the Comptoir Lyon Alemand Louyot and then rolled to 0.13 mm thick foils. Then, 3 mm diameter discs were punched out from the foils.

All samples were annealed for 24 h at 1000°C to eliminate dislocations mainly coming out of cold work and then put into stainless steel containers adapted to high pressure tritium handling. Samples were activated

* Corresponding author. Tel.: +33-1 49 78 12 14; fax: +33-1 49 78 12 03.

E-mail address: decamps@glvt-cnrs.fr (B. Décamps).

0022-3115/00/$ - see front matter
PII: S0022-3115(99)00191-9

by heating at 150°C under dynamic secondary vacuum for 48 h before tritium charging.

Tritium absorption was done at room temperature under a 10 bars pressure for all specimens (Pd, $Pd_{90}Rh_{10}$ and $Pd_{90}Pt_{10}$). The amount of absorbed tritium was estimated from the exact pressure left in the container. Aging was done at room temperature and the helium amount in the sample was deduced from both the initial tritium content and the aging time, assuming that all ^{3}He generated in the solid is retained. Tritium was removed by isotopic exchange with deuterium at room temperature, keeping samples in the β phase (to avoid numerous $\alpha \leftrightarrow \beta$ phase transitions which would create a great density of dislocations). The gas ($D_2 + T_2$) was removed from the container and samples were kept under dynamic secondary vacuum always at room temperature for 48 h, so samples eventually experienced a complete $\alpha \leftrightarrow \beta$ phase transition cycle.

In order to determine the influence of $\alpha \leftrightarrow \beta$ phase transitions on the samples microstructure, a Pd sample was thinned before tritium absorption and observed before and after aging. In this case, the tritium absorption was done above the miscibility gap of Pd–T_2 system, at 300°C and 80 bars, to avoid the first $\alpha \rightarrow \beta$ phase transition. The sample was aged at room temperature and tritium was removed by isotopic exchange, as described previously. The final gas desorption was done at room temperature to avoid a ^{3}He reorganization (usually induced by high temperature treatments) but the sample experienced a $\beta \rightarrow \alpha$ transition. Eventually, to distinguish the effect of $\beta \rightarrow \alpha$ transition from the aging effect, a Pd sample was prepared in the same conditions as described above, but with D_2 instead of T_2.

Discs were thinned down by jet-electropolishing using a 70 vol% acetic acid and 30 vol% perchloric acid electrolyte kept at room temperature under 30 V to be observed by TEM. In order to check the presence of possible artifacts induced by the electropolishing, some specimens have been thinned using ion beam milling.

Remark: In a first attempt, the aging was performed on Pd thin slices previously mapped by TEM but due to a strong deformation of the specimen, the aging has been done for all alloys on bulk specimens thinned just before observation as described above.

2.2. TEM techniques

Conventional bright field [7] and weak beam dark field [8] observations are performed in a JEOL 2000EX TEM.

High resolution images are taken in a JEOL 4000EX TEM using thickness and defocus conditions in which the atomic columns are bright.

For the visualization of He bubbles, special imaging conditions are used [9]. The specimen is oriented far from any Bragg conditions and large through-focus series (between −300 and +300 nm) are taken in order to reveal the presence of the bubbles. For negative defocus (underfocus of the objective lens), they appear as white dots surrounded by a dark fringe while for positive defocus (overfocus), the dots are black and the fringe is white. No particular contrast is observed close to the exact focus position. The size of the bubbles has been estimated by measuring the size of the dot in the through-focus series.

Image simulation is performed using the commercial multislice EMS program [10]. Image of voids is done using the following parameters: spherical aberration coefficient = 1.05 mm, beam divergence = 0.8 mrad, defocus spread = 9 nm, Debye–Waller factor = 0.0034 (Pd), 0.05 (He) and absorption coefficient = 0.06 (Pd), 0.01 (He). For high resolution images, the value of the objective aperture is 12 nm^{-1} while it is equal to 2 nm^{-1} for the imaging of the bubbles.

The determination of the bubble density is done by using an automated procedure which has already been described [11]. The experimental images are first filtered with an annular mask to remove low and high spatial frequencies. Then the local intensity maxima (or minima) are detected and numbered giving the bubble density. The procedure is done on both dark and white contrast of the bubbles and it has been verified that the density measurements give the same results using both contrasts. The density results are also compared to purely manual measurements. The density measurement needs the determination of the specimen thickness. This has been performed using two beam bright field images presenting thickness fringes.

3. Experimental results

3.1. TEM observations

3.1.1. Palladium

(1) *Annealed samples*: After annealing, a few small perfect dislocation loops (mean size about 6 nm) and dislocations are already present in the sample.

(2) *Tritiated samples*: TEM observations have been performed on Pd samples aged during 1, 2 and 3 months, respectively. Even after one month of aging (Fig. 1(a)), the density of defects is important leading to a very difficult analysis of these defects. This high density of defects is correlated to an important deformation of the thin foil. TEM bright field pictures then show a great density of small defects, which appear either as single black dots (noted BD on micrographs) or as black and white contrast typical of interstitial or vacancy agglomeration defects. In the past, black dots (range of 1–2 nm) produced by neutron or electron irradiation experiments have been extensively studied in the literature and were identified as small dislocation loops. One

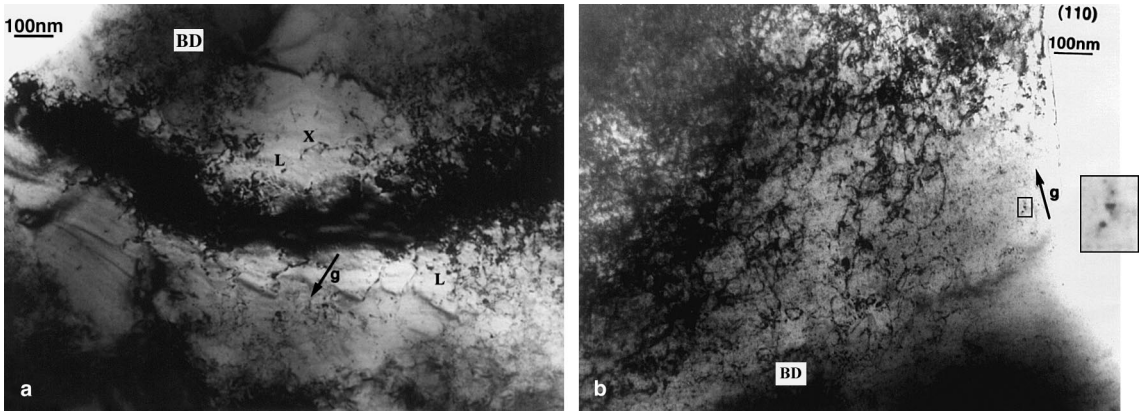

Fig. 1. Bulk palladium after aging: (a) bright field micrograph after one month of aging, $g = \langle 2\,0\,0 \rangle$; (b) bright field micrograph after two months of aging, $g = \langle 1\,1\,1 \rangle$. BD = black dots; L = perfect dislocation loop; X = black dot on a dislocation.

of these defects is shown in the insert of Fig. 1(b): the value of the angle between the reflexion vector and the black/white contrast line is consistent with that given by an imperfect dislocation loop (Frank loop). However, in our samples, defect size is smaller than the weak beam technique resolution, so it is not possible to clearly analyze them. As in the treatment undergone by the specimen no vacancy production is expected, these defects, some of them being experimentally identified as dislocation loops as shown in Fig. 1(b), may correspond to clusters of self-interstitial atoms (CSIA). Some of these defects are located on dislocations: this is already visible after the first month of aging as shown in Fig. 1(a) (part X). A few perfect dislocation loops (mean size about 6 nm) and quite numerous dislocations are visible. When the duration of aging is increased, the density of dislocations and CSIA also increases, while that of perfect dislocation loops remains very low. An accurate measurement of these densities is nevertheless not possible due to an inhomogeneous distribution. After three months, the dislocation structure is almost hidden by the density of CSIA.

The presence of He bubbles has been revealed using through-focus experiments. An example is given in Figs. 2(a) and (b) for three-months aging. The size of the bubbles using direct measurement is close to 1 nm. The study of the different images of the through-focus series shows that the width of the bubble images is not sensitive to the exact defocus value. However, the contrast itself depends on this value. The highest contrast is obtained in the defocus range: 150–300 nm (positive or negative). The contrast is also very sensitive to the presence of a contamination layer on the surfaces of the specimen. HRTEM observations on three-months aged samples reveal also the presence of ^{3}He bubbles (Fig. 3(a)). They appear as a small brighter region. It is to be noticed that no deformation of the atomic planes bordering the bubble is visible which is in agreement with the contrast given by the conventional overfocus/underfocus images. There is no elastic deformation field around the bubbles. The density of the bubbles is in the range of $0.3–1 \times 10^{25}$ bubbles/m^3. Comparing the three aging times, it appears that although the bubbles density seems to increase with time of aging, the measured

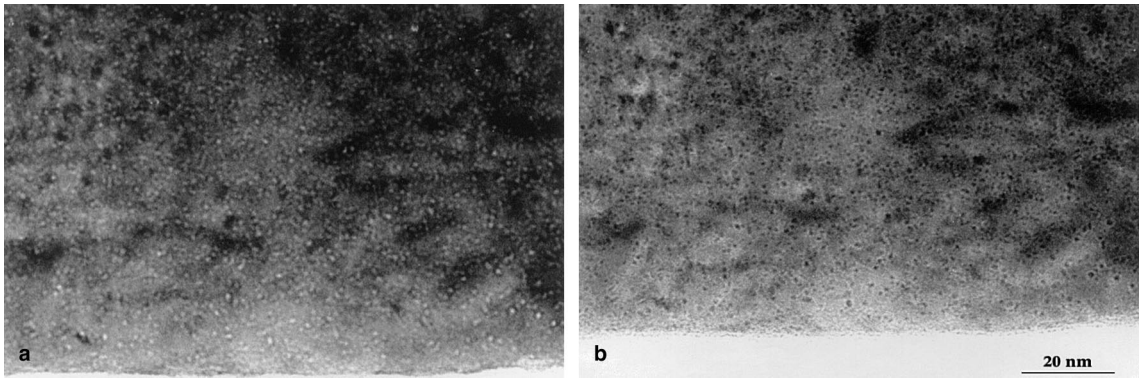

Fig. 2. Bright through-focal series of He bubbles in Pd after three months of aging: (a) underfocus, (b) overfocus.

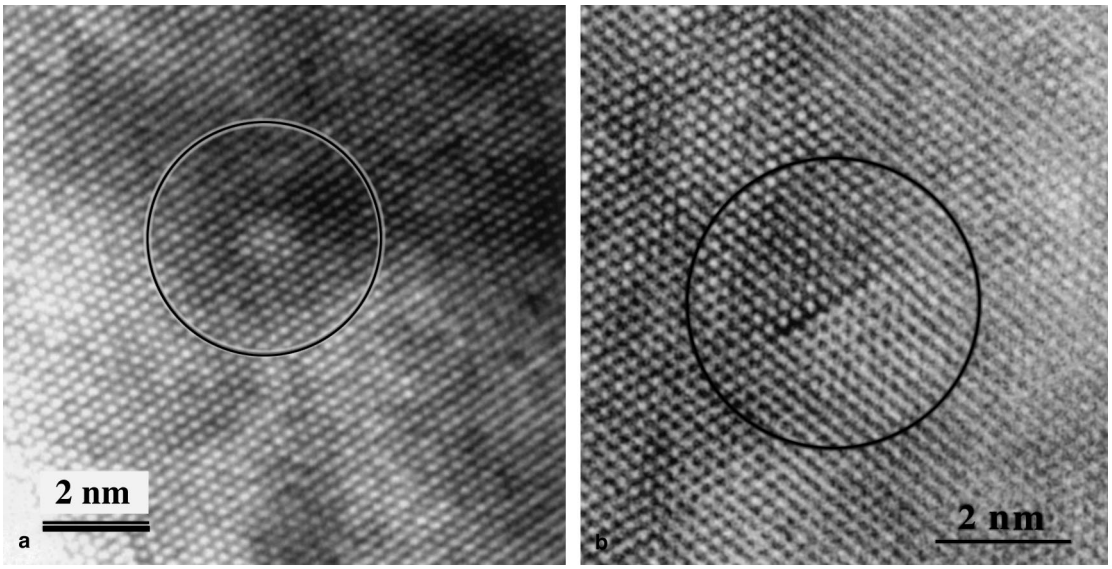

Fig. 3. Bulk palladium after three months of aging: (a) high resolution image showing a He bubble; (b) high resolution image showing an interstitial defect.

increment is within the error bar. This is due in particular to a difficulty to assess the exact thickness of the specimen.

High resolution reveals also the presence of small defects lying in the {1 1 1} planes as shown in Fig. 3(b). These defects, introducing a lattice deformation and presenting an interstitial character, correspond to Frank interstitial loops. Due to their size (around 1.3 nm) and their interstitial character, they can be attributed to CSIA.

(3) *Deuterated samples*: In this case, the deformation of the samples is of the same order as for tritiated samples and the precise analysis of the defects is not possible because of the bad diffracting conditions due to lattice distortion. As the specimen was not tritiated, we conclude that the deformation is due to gas absorption and/or desorption more than aging. The main point is that these deuterated samples never exhibit similar defects (CSIA, He bubbles) to those revealed by TEM in the tritiated specimens.

This clearly demonstrates that CSIA and bubbles are really characteristics of palladium-tritiated aged samples.

3.1.2. Palladium alloys

3.1.2.1. Characterization of the defects.

$Pd_{90}Rh_{10}$. (1) *Annealed samples*: In this case, the annealed samples show a low density of dislocations including perfect loops which is very similar to what has been observed for pure Pd.

(2) *Tritiated samples*: Generally, the deformation of tritiated $Pd_{90}Rh_{10}$ samples is smaller than that of Pd samples but due to the similarity between the two materials, no micrograph will be presented for the alloy. $Pd_{90}Rh_{10}$ samples aged for 1, 2 and 3 months have been observed by TEM. After one month of aging, a great density of dislocations is evidenced together with a few perfect dislocation loops (mean size around 6 nm) and a small density of CSIA. After two months, the density of both dislocations and CSIA increases and pictures are similar to Pd's for the same duration of storage. After three months, dislocations are totally hidden by clusters of SIA, similar to the observations made in Pd samples.

Here again, it can be concluded that the increasing density of dislocations and CSIA is due to aging.

$Pd_{90}Pt_{10}$. (1) *Annealed samples*: The microstructure of annealed samples shows an important density of rectangular dislocation loops (density about 10^{19} loops/m^3 and mean size around 200 nm) located in {1 0 0} planes. Similar loops are also reported in specimens thinned down by ion bombardment techniques.

(2) *Tritiated samples*: First of all, we notice that $Pd_{90}Pt_{10}$ samples are almost not deformed by the different treatments. After one month (Fig. 4(a)), a great density of very small (less than 20 nm diameter) faulted rectangular dislocation loops appears in the observed sample while larger ones are still present (density in the range of 2–4 10^{20} loops/m^3). These dislocation loops are similar to those encountered after annealing. They are located in {1 0 0} planes. They are shown to be out of contrast for $g=\langle 2\,0\,0\rangle$. The analysis using $g.b=0$ conditions and simulations with the PCTWO program [12] demonstrates that their Burgers vector is perpendicular to the loop plane and has a very small magnitude (between $a/5$ and $a/7$ $\langle 1\,0\,0\rangle$). High resolution observations confirm also this result as shown in Fig. 4(b)).

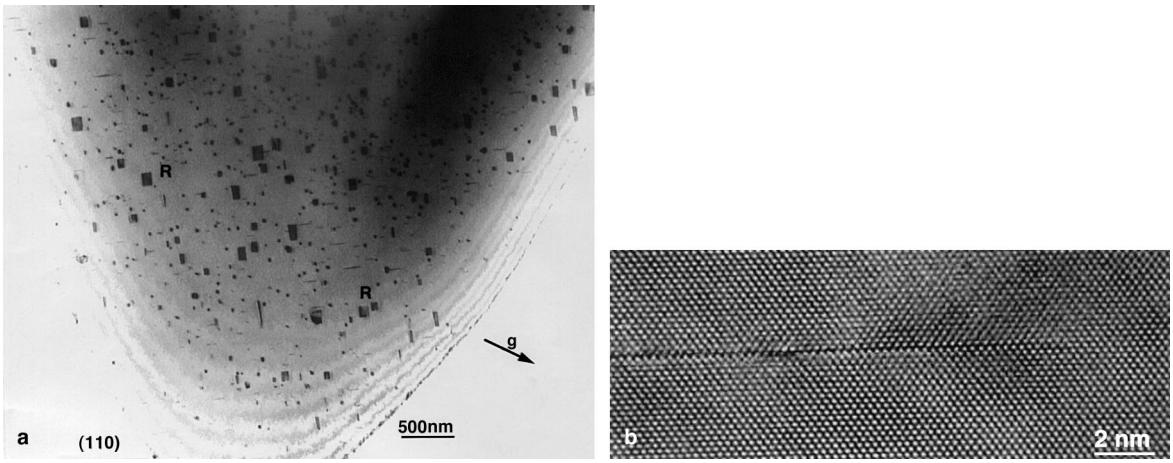

Fig. 4. Bulk $Pd_{90}Pt_{10}$ after one month of aging: (a) bright field micrograph, $g = \langle 1\,1\,1 \rangle$. R is the faulted rectangular loop; (b) high resolution micrograph.

After two months of aging, these small loops tend to disappear; consequently the dislocation loops' density seems to decrease. Samples still do not contain dislocations but a few CSIA appeared. After three months, the very small loops reported after one month of aging are absent and the density of the dislocation loops seems to be of the same order as that observed after two months of aging. The density of CSIA becomes important.

So, it seems that faulted dislocation loops are usual defects in these $Pd_{90}Pt_{10}$ samples. Aging seems to induce first the apparition of a great density of very small loops that disappear during further aging.

3.1.2.2. Helium bubbles. In all the alloys, He bubbles are present and the results concerning their size and density are summarized in Table 1 in comparison to pure Pd.

3.2. Simulation of the bubble contrast

In order to check the visibility conditions of the bubbles, image simulations have been performed in the two observation modes: high resolution and conventional white or dark contrast. In the high resolution mode, the objective aperture diameter is equal to 12 nm^{-1}, while a 2 nm^{-1} is used in the conventional mode. The influence of several parameters has been investigated in detail: presence (or absence) of helium atoms, thickness of the specimen and depth of the bubble within the specimen. As it has already been shown experimentally, the bubbles do not induce elastic deformation in the matrix. Two models have been constructed: the first one contains an empty void located at the center of the specimen. The shape is roughly spherical and the radius is equal to 0.5 nm. No deformation is present around the cavity. In the second model, the cavity is filled by helium atoms each of which occupy a 15 $Å^3$ volume. In this model, Pd atoms inside the bubble have all been replaced by helium atoms located at the same position. Above and below the cavity, slices of pure palladium are present. By changing the total number of these slices and their proportion above and below the cavity, the effect of the total thickness as well as the position of the cavity within the thin foil can be investigated. Two thicknesses have been simulated: 6.5 and 12 nm corresponding, respectively, to 10 and 20 palladium slices on each side of the cavity. The effect of the relative depth has been investigated only for the 6.5 nm thickness: three depths corresponding to: 5 slices above and 15 slices below the cavity, 10 slices on each side and 15 slices above and 5 below have been calculated. All the images have been calculated using the experimental parameters corresponding to the 4000EX microscope.

Table 1
Bubble density and size for palladium and its alloys

Alloy	Density (bubbles/m^3)	Average size (nm)
Pd	$0.3–1\times10^{25}$	1
$Pd_{90}Rh_{10}$	$0.3–1\times10^{25}$	1
$Pd_{90}Pt_{10}$	$0.3–1\times10^{25}$	0.8

High resolution imaging: Although extended through-focus series have been calculated, the contrast measurements have been done using the focus conditions giving white palladium atomic positions in agreement with most of the experimental images. The results can be summarized as follows:

- The bubble gives rise to a detectable contrast in which some atomic positions appear brighter than the surrounding matrix. The extension of this contrast is smaller than the actual size of the bubble (Fig. 5). This could be due to the model shape and the estimation of the thickness of the foil.

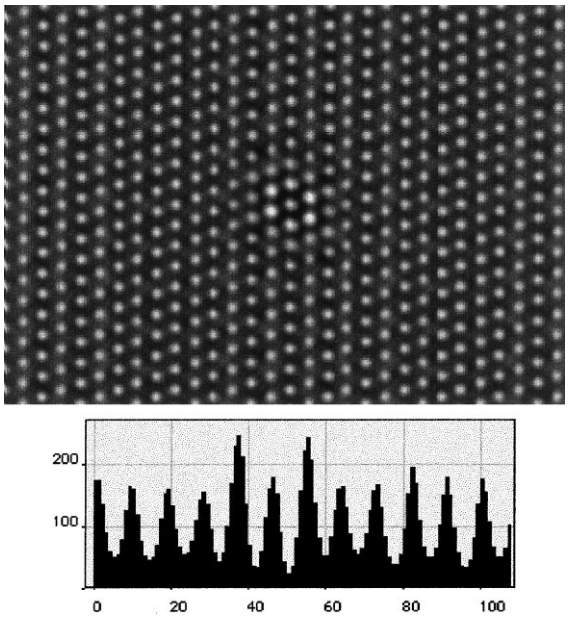

Fig. 5. High resolution simulated image of an empty cavity with the intensity profile.

- The presence of helium atoms does not induce a detectable change in the contrast. This can be explained by the low scattering factor of helium atoms compared to palladium one.
- The contrast decreases as the total thickness increases. The bubble becomes hardly detectable when the thickness reaches 12 nm.
- The contrast is affected by the position of the bubble in the specimen thickness. It increases when the bubble is close to the lower surface of the specimen.

Conventional imaging: Only a centered He bubble in a 6.5 nm thick specimen has been calculated. In this case, large defocus values have been used. Fig. 6(a)) and (b) show the resulting contrast. In agreement with experimental images, the bubble appears as a white dot if a negative defocus value is used and is reversed if the defocus becomes positive. The total contrast (dot plus fringe) is larger than the size of the cavity. This is probably due to the fact that the fringes are located on the outside of the defect. It is to be noted that the size of the dot is similar to that of the cavity.

4. Interpretation and discussion

The TEM images show that after aging, all the specimens contain helium bubbles, dislocations, dislo-

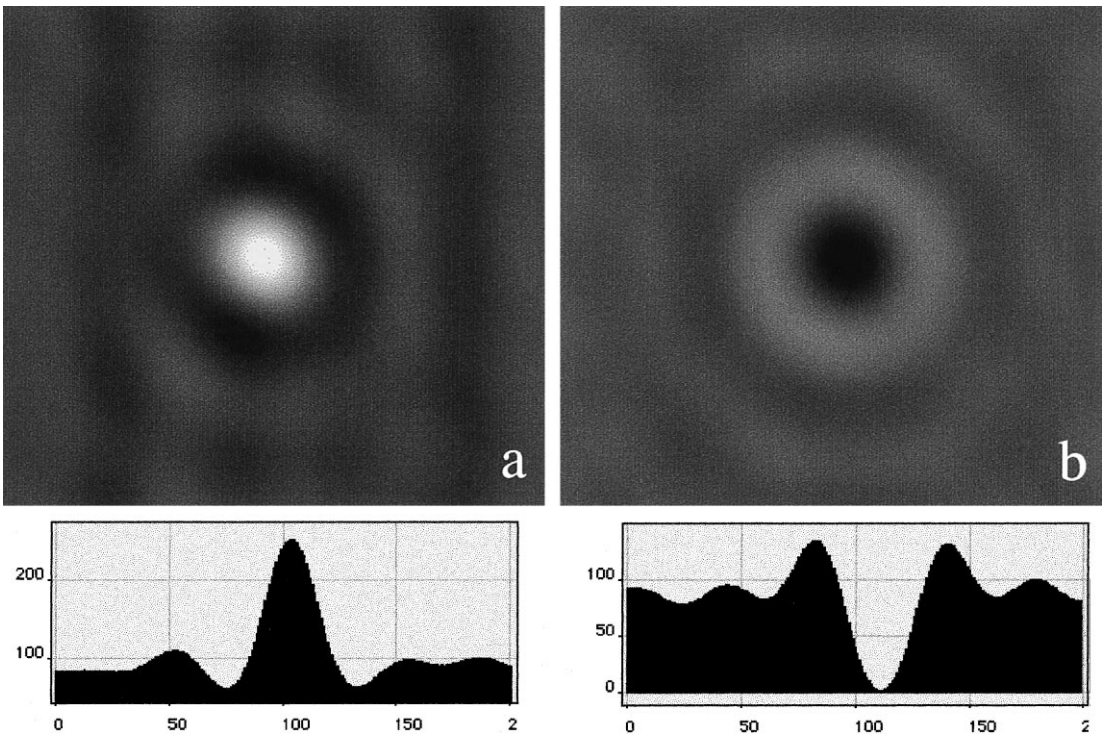

Fig. 6. Simulation of through-focal images of a He bubble with intensity profiles: (a) underfocus $\delta z = -150$ nm, (b) overfocus $\delta z = +150$ nm.

cations loops and agglomerated interstitial defects (clusters of self-interstitial atoms – CSIA). Due to their very small size (<3 nm), these last defects could not be characterized in detail using the weak beam technique. Nevertheless, their contrast is consistent with interstitial Frank loops. Their interstitial character has been put into evidence using high resolution experiments. Due to their inhomogeneous repartition, it has not been possible to estimate their density.

For all specimens, perfect dislocation loops are already present in the non-aged specimen and their role during aging is not clear. This point will be discussed later. Their number is difficult to evaluate.

Concerning the helium bubbles, the observations show their presence in all the specimens whatever the aging time (one to three months). The mean size of the bubbles is $d = 1 \pm 0.2$ nm for Pd and $Pd_{90}Rh_{10}$ and 0.8 ± 0.2 nm for $Pd_{90}Pt_{10}$. This size does not change with the aging time (in the range of one to three months). This determination of the mean size of the bubbles has been performed on experimental through-focus bright field images as shown before. These bubbles have also been identified in high resolution. A cavity model (empty or filled with helium) has been used for computation. As the mean size of the bubbles has been determined by measuring the size of the dots on the bright field images, the obtained value is a good assessment of the real one according to the computation. Nevertheless, in high resolution, the simulated contrast is smaller than the size of the model. This is probably due to the model shape and the estimation of the foil thickness. The density is in the range of $0.3–1 \times 10^{25}$ bubbles/m^3 (for three months of aging) and if this density seems to increase with the aging time, the value is still within the error bar due to thickness evaluation. This bubble density is slightly higher than previous measurements by Thomas and Mintz [4] on Pd after two months of aging ($5–10 \times 10^{23}$ bubbles/m^3 and average diameter around 1.5–2 nm) although the bubble size is smaller in our case. From the mean size and the density of the bubbles, the total number of helium atoms can be evaluated if the volume occupied by a helium atom is known. A value of 8 Å^3 for the volume requirement of a ^{3}He atom in a bubble has been established in the literature [13–15] for different tritides (Lu, Nb, Pd and Ta) and is since used as a reference for this type of study. Using this value, the proportion He/M has been calculated for the three alloys after three months of aging and compared to the experimental value. The calculation has been performed assuming an occupancy of four metallic atoms per unit cell. The upper value of the bubble density has been taken in order to compensate the difference of size between experimental and simulated high resolution images. It can be shown that mainly all the helium is localized within the bubbles after three months of aging for the three alloys. As an example for Pd alloys the values are the following: He/Pd (experimental) = 0.99; V (Pd atom) = 14.7 Å^3; bubble density = 10^{25} bubbles/m^3; He/Pd (calculated) = 0.96. A similar calculation may be done on the density determinations performed by Thomas and Mintz [4] estimating the proportion He/M [16]. The result is identical despite the difference in density and bubble size, all the helium is localized within the bubbles. This repartition of the helium in the material is generally expected in the literature after such time of aging. Nevertheless, this value of 8 Å^3 requires a very high pressure within the bubbles (range 6–11 GPa for Pd tritides [13,14]). Our experimental results reveal that there is no detectable elastic field around the bubbles. This is clearly put into evidence on high resolution images. Numerical simulations performed by Cochrane and Goodhew [17] demonstrate that a gas pressure of between 0.5 and 0.75 GPa must be present in overpressurized bubbles for significant strain contrast to be observed. Knowing the range of pressure in the bubbles, the volume requirement for a ^{3}He atom within the bubble can be obtained from the formula established by Le Toullec, Loubeyre and Pinceaux [18]. Pressure between 0.5 and 1 GPa leads to atomic volume in the range of 23–17 Å^3. These values are two to three times higher than the value usually taken in the literature (8 Å^3). This would demonstrate that after three months of aging, only a fraction of the helium is localized within the bubbles.

Another point to discuss is the growth mechanism of these bubbles. At room temperature, they grow by an athermal mechanism involving the formation of self-interstitial atoms and/or dislocation loop punching. This last mechanism requires high pressure within helium bubbles. This pressure has been estimated by Greenwood et al. [19] to be of the order of $\mu b/r$. The application of this formula to the palladium gives a pressure of the order of 24 GPa ($\mu = 43.6$ GPa, $b = 0.27$ nm, $r = 0.5$ nm). It is to be noted that for rhodium and platinum, the corresponding values are respectively, 150.4 and 61.2 GPa for μ. As we are dealing with solid solutions, the corresponding values for the alloys can be approached by linear approximation. This demonstrates that the value of 24 GPa is the lowest limit for the calculated pressure within the bubble. However, extreme care must be taken in the application of the Greenwood et al. formula to very small loops. Nevertheless, this demonstrates that the mechanism of bubble growth involving dislocation loop punching does not operate in our alloys up to three months of aging. From the experimental point of view, it has not been possible to determine if this mechanism was operating or not for the following reasons:

- perfect dislocation loops (mean size 6 nm) have been observed before and after aging.
- Due to the very small size of the helium bubbles, if dislocation loops were emitted, their size would prob-

ably be similar to that of the bubbles which means similar to CSIA. So, it would not be possible to distinguish them.

Nevertheless, due to the high value of the pressure required for this mechanism to operate with respect to that estimated within our bubbles, it can be assumed that the bubbles grow by a mechanism involving the formation of CSIA. This is experimentally confirmed in our alloys by the increase of the CSIA density with the aging time.

A comparison between the effect of the different substitution elements has also been performed.

Palladium and palladium–rhodium alloys have a very similar behavior: the density of defects (dislocations and CSIA) increases with the aging time. Already after one month of aging, the lattice deformation is very significant with the formation of a dislocation network. Clusters of SIA are clearly visible and some of them are attached to dislocations. Upon aging, the density of dislocations and CSIA increases quickly. After three months of aging, the dislocation network is hidden by the CSIA.

The case of the palladium–platinum alloy is different: the density of defects is much smaller and the induced deformation is also smaller. The lattice is almost not deformed during aging. Very few dislocations are visible even after three months of aging. The formation of clusters of SIA is observed and they are homogeneously distributed within the sample. The point to discuss is the presence of rectangular faulted loops after the first annealing of the specimen together with their evolution upon aging. The nature of these loops is very peculiar for an FCC alloy: they are located on $\{1\,0\,0\}$ planes and the magnitude of their Burgers vector is in the range of $a/5$–$a/7$ $\langle 1\,0\,0\rangle$. The origin of these loops needs to be better understood and further experiments are required to clarify this point. The hypothesis of Guinier–Preston zones has also to be considered. Nevertheless, the hypothesis of electrochemical processes can be put aside as ion bombardment thinning leads to similar observations. After one month of aging, small loops (diameter <20 nm) have been reported while after two and three months of aging, they seem not to be present. This could be related to aging mechanisms.

In order to interpret the behavior of these palladium-based alloys during aging, it is necessary to compare our results to those obtained on the same alloys (Pd, $Pd_{90}Rh_{10}$ and $Pd_{90}Pt_{10}$) using complementary techniques like X-ray and neutron scattering experiments [20].

The evolution of Debye–Scherrer lines indicates the nature and density of defects created by ^{3}He bubbles formation: finite size defects (such as isolated SIA, clusters of SIA and dislocation loops) induce a shift of the peaks towards small angles, i.e., an increase of lattice parameters, while infinite size defects (such as dislocations) induce a broadening of the peaks [21].

In the case of Pd, the X-ray study showed that, during the first three months, the lattice parameter increased very quickly, indicating that a great density of finite size defects was created. During the next three months, the lattice parameter increase progressively slowed down and, after six months of aging, the lattice parameter remained almost constant. As SIA were continuously generated, it has been assumed that, at this stage of aging, new SIA were incorporated to a dislocations network. Neutron scattering experiments showed that a great density of dislocations was created in Pd during the first two weeks, which means that a part of the SIA was immediately integrated to the dislocation network, while the other part remained as isolated defects. As the time of storage was raised, the ratio of SIA incorporated to the dislocations structure increased. TEM experiments confirmed these results: a great density of dislocations was evidenced after only one month of aging and this density increased with the time of storage. It was also possible, by TEM, to identify the finite size defects as CSIA. The incorporation of CSIA into the dislocation network has been evidenced.

It has also been shown (X-ray and neutron scattering experiments [20]) that substitution by rhodium has little effect on the evolution of structural properties during aging: the increase of the lattice parameter was slightly more important, at the same ^{3}He concentration, in $Pd_{90}Rh_{10}$ than in pure Pd, while the peak broadening was of the same order in the two materials. By TEM, we also observed the same behavior for $Pd_{90}Rh_{10}$ than for pure Pd: a density of dislocations, of the same order, was visible after only one month of storage, and finite volume defects were identified as CSIA.

On the contrary using X-ray and neutron scattering experiments [20], it has been shown that substitution by platinum has a great influence on aging phenomena. First, the increase of the lattice parameter was greater and faster for $Pd_{90}Pt_{10}$ than for Pd, which has been attributed to the fact that more SIA remain as finite volume defects. Consequently, less dislocations are created and a very small broadening of diffraction peaks during the first months of aging has been observed. These hypotheses were confirmed by TEM: $Pd_{90}Pt_{10}$ samples contained very few dislocations, even after three months of aging. Nevertheless, a great density of small faulted dislocation loops was evidenced in the $Pd_{90}Pt_{10}$ samples that could be assumed to be responsible for the lattice parameter increase. So, here again, TEM allowed to identify the nature of finite size defects as small dislocation loops.

Although there is no clear explanation for the different behavior of the palladium–platinum alloy, atomic size or electronic structure effects may be invoked and work will be undertaken in the near future in this way.

5. Conclusions

A combination of TEM techniques has been used to study the evolution under aging of different palladium tritides (Pd, $Pd_{90}Rh_{10}$ and $Pd_{90}Pt_{10}$). The main results are the following:

- He bubbles have been identified for all aging times and metallic substitution in bright field conventional and in high resolution imaging. Their density is in the range of $0.3–1\times10^{25}$ bubbles/m^3 and the size varies from 0.8 nm ($Pd_{90}Pt_{10}$) to 1 nm (Pd and $Pd_{90}Rh_{10}$). It has been shown that there is no deformation of the atomic planes bordering the bubbles. On this basis, an estimation of the higher limit pressure within the bubbles can be performed (< 0.5–0.75 GPa) and thus the volume requirement for a ^{3}He atom can be estimated. This volume is significantly higher (23–17 $Å^3$) than the reference value taken in the literature (8 $Å^3$) which indicates that only a fraction of the helium could be located within the bubbles.
- Our work also demonstrates that the mechanism of bubble growth involving dislocation loops punching does not operate due to this low value of the pressure within the bubbles. For these alloys, the mechanism implying the formation of CSIA is predominant. For $Pd_{90}Pt_{10}$, the presence of faulted loops and their evolution upon aging has been evidenced.
- These results give a direct proof to the aging models which have been proposed on the basis of X-rays and neutron diffraction experiments with a measure of the size of the defects formed (clusters of self-interstitial atoms, dislocation loops and helium bubbles) together with their evolution under aging.

References

[1] T.B. Flanagan, W.A. Oates, Ann. Rev. Mater. Sci. 21 (1991) 269.
[2] Y. Fukai, The Metal Hydrogen System, Springer, Berlin, Heidelberg, 1992.
[3] W. Jager, R. Lasser, T. Schober, G.J. Thomas, Radiat. Eff. 78 (1983) 165.
[4] G.J. Thomas, J.M. Mintz, J. Nucl. Mater. 116 (1983) 336.
[5] T. Schober, R. Lasser, W. Jager, G.J. Thomas, J. Nucl. Mater. 122&123 (1984) 571.
[6] T. Schober, G.J. Thomas, R. Lasser, W. Jager, Scr. Metall. 18 (1984) 255.
[7] P.B. Hirsch, A. Howie, R.B. Nicholson, D.W. Pashley, M.J. Whelan, Electron Microscopy of Thin Crystals, Krieger, New York, 1977.
[8] D.J.H. Cockayne, I.L.F. Ray, M.J. Whelan, Philos. Mag. 20 (1969) 1265.
[9] M.J. Loretto, R.E. Smallman, Defect Analysis in Electron Microscopy, Wiley, New York, 1975.
[10] P. Stadelmann, Ultramicroscopy 21 (1987) 131.
[11] B. Decamps, J.M. Penisson, S. Thiebaut, A. Percheron Guegan, in: Proceedings of the 14th International Congress on Electron Microscopy Cancun, vol. 3, ICEM 14, Symposium GG, 1998.
[12] A.K. Head, P. Humble, L.M. Clarebrough, A.J. Morton, C.T. Forwood, Computed Electron Micrographs and Defects Identification, North-Holland, Amsterdam, 1973.
[13] G.C. Abell, A. Attalla, Phys. Rev. Lett. 59 (9) (1987) 995.
[14] G.C. Abell, A. Attalla, Fus. Technol. 14 (1988) 643.
[15] T. Schober, C. Dieker, R. Lasser, H. Trinkaus, Phys. Rev. B 40 (2) (1989) 1277.
[16] S. Thiebaut, thèse de l'Université Paris VI, 1996.
[17] B. Cochrane, P.J. Goodhew, Phys. Status Solidi A 77 (1983) 269.
[18] R. Le Toullec, P. Loubeyre, J.P. Pinceaux, Phys. Rev. B 40 (4) (1989) 2368.
[19] G.W. Greenwood, A.J.E. Foreman, D.E. Rimmer, J. Nucl. Mater. 4 (1959) 305.
[20] S. Thiebaut, V. Paul-Boncour, A. Percheron Guegan, B. Limacher, O. Blaschko, C. Maier, C. Tailland, D. Leroy, Phys. Rev. B 57 (17) (1998) 10379.
[21] M.A. Krivoglaz, Theory of X-ray and Thermal Neutron Scattering by Real Crystals, Plenum, New York, 1969.